ACS APPLIED MATERIALS & INTERFACES

Research Article

www.acsami.org

In Situ Formation of ZnO in Graphene: A Facile Way To Produce a Smooth and Highly Conductive Electron Transport Layer for Polymer Solar Cells

Aifeng Hu,[†] Qingxia Wang,[†] Lie Chen,[†,‡] Xiaotian Hu,[†] Yong Zhang,[†] Yinfu Wu,[†] and Yiwang Chen*[,†,‡]

[†]College of Chemistry/Institute of Polymers, Nanchang University, 999 Xuefu Avenue, Nanchang 330031, China

[‡]Jiangxi Provincial Key Laboratory of New Energy Chemistry, Nanchang University, 999 Xuefu Avenue, Nanchang 330031, China

Supporting Information

ABSTRACT: A novel electron transport layer (ETL) based on zinc oxide@graphene:ethyl cellulose (ZnO@G:EC) nanocomposite is prepared by in situ formation of zinc oxide (ZnO) nanocrystals in a graphene matrix to improve the performance of polymer solar cells. Liquid ultrasound exfoliation by ethyl cellulose as stabilizer not only allows for uniform dispersion of graphene solution but also maintains an original structure of graphene gaining a high conductivity. The ZnO@G:EC ETL displays a quite smooth morphology and develops the energy-level alignment for the electron extraction and transportation. Subsequently, the device based on poly(3-hexylthiophene) (P3HT):(6,6)-phenyl-C_{61} butyric acid methyl ester ($PC_{61}BM$) with the ZnO@G:EC as ETL obtains a power conversion efficiency (PCE) of 3.9%, exhibiting a ~20% improvement compared to the familiar device with bare ZnO nanocrystals as ETL. Replacing the active layer with polythieno[3,4-*b*]thiophene/benzodithiophene (PTB7): (6,6)-phenyl-C_{71} butyric acid methyl ester ($PC_{71}BM$), the PCE can be dramatically improved to 8.4%. This facile and fascinating method to produce a smooth and highly conductive electron transport layer provides an anticipated approach to obtain high performance polymer solar cells.

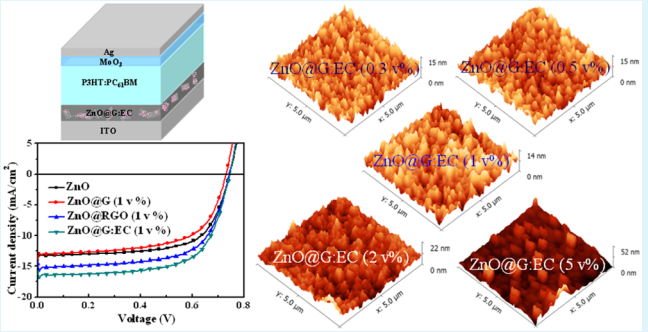

KEYWORDS: *graphene, cellulose, polymer solar cells, electron transport layer, nanocomposites*

INTRODUCTION

Polymer solar cells (PSCs) have been attracted considerable interest due to their being lightweight and having low cost and easily printable nature with mechanical flexibility. The power conversion efficiency (PCE) of PSCs has achieved 10.6%,[1] and a further breakthrough is still being pursued today. Generally, there are two typical types of device architectures: conventional and inverted structures. The conventional structure usually consists of a low work function metal cathode, an electron transport layer (ETL), an active layer, a popular hole transport layer, poly(3,4-ethylenedioxythiophene):poly(styrenesulfonate) (PEDOT:PSS),[2] and an indium tin oxide (ITO) anode. But the stability and PCE of this device structure are rapidly attenuated for the acidic PEDOT:PSS corroding ITO and easily oxidized cathode (aluminum).[3−5] To relieve these problems, the inverted structure with a high work function metal anode (argentum) and ITO cathode coating an n-type material (such as zinc oxide) is of particular interested. As a result, compared with a conventional device, the inverted structure device shows a higher stability to ambient.[3,6] Currently, although the development of an original active material plays a significant role in obtaining a breakthrough PCE, the modifications to the interface between the active layer and electrodes cannot be underestimated. It is well-known that a desirable interface interlayer can tune the energy level[7,8] and improve the interfacial stability between the active layer and electrodes,[6,9] as a result of a promotion to the device performance.

As a rule, electron transport layers (ETLs) included organic materials (such as poly[(9,9-bis(3′-(*N*,*N*-dimethylamino)-propyl)-2,7-fluorene)-*alt*-2,7-(9,9-dioctylfluorene)] (PFN),[1] poly(ethylene oxide)) and inorganic metal oxide materials (for instance, lithium fluoride (LiF),[10−12] titanium oxide (TiO_x),[8,13,14] zinc oxide (ZnO)[7,9,13,15−17]). Therein, ZnO is mainly employed as the ETL of inverted PSCs, owing to its higher electron mobility,[18] favorable optical transparency,[19] and nontoxicity. However, the device performance of the ZnO based ETL is limited because of an uneven spatial distribution of the nanocrystals on a large area,[20,21] high annealing temperatures (≥200 °C),[22,23] incompatibility with ITO substrates,[22] and the fact that its conductivity[24−26] also needs to be improved. So far, there are two primary techniques, including solvent treatment[7,27,28] and chemical modification[13,29] of the ZnO based ETL, that are used in the processing of the interface engineering to resolve these problems. The

Received: May 27, 2015
Accepted: July 6, 2015
Published: July 6, 2015

DOI: 10.1021/acsami.5b04555
ACS Appl. Mater. Interfaces 2015, 7, 16078−16085

solvent treatment technique was restricted for its application to only a few specific ZnO based ETLs. However, the chemical modification is given more attention due to a more universal application. It has been verified that a chemical modification of ZnO with carbon nanomaterials, such as graphene, graphene oxide (GO),[30,31] reduced graphene oxide (RGO)[13,16,32,33] and carbon nanotubes (CNT),[31] could act as an effective ETL to improve the device performance. Among these carbon nanomaterials, graphene has attracted widespread interest for its two-dimensional (2D) planar structure and excellent electrical conductivity.[34] Unfortunately, it is difficult to disperse pristine graphene in precursor solutions ascribed to the strong π-stacking interactions between graphene sheets. So the GO is regarded as a preferable substitution for its excellent dispersion. While it is restrained for a poor conductivity because of the abundant oxygen functional groups, therefore the GO film always needs to be treated through thermal reduction or chemical reduction to obtain RGO for practical application. However, the obtained RGO from the sophisticated technique probably tends to aggregate again, and the reduction degree of the GO is also uncertain. In light of our previous work, poly(*N*-vinylpyrrolidone) (PVP) stabilized RGO was used to modify ZnO as electron transport layer, achieving better device performance.[32] Nevertheless, it is surprising that the reduction degree of the GO was insufficient to further impede improvement of PCE. Therefore, it is necessary to find a superior way to prepare graphene with high dispersion and conductivity to modify ZnO as an ETL for improved PSCs efficiency.

Herein, highly dispersed graphene sheets, instead of RGO, are directly employed to modify ZnO for improving the PSC performance. A novel ZnO@graphene:ethyl cellulose (ZnO@G:EC) nanocomposite is prepared by in situ formation of ZnO nanocrystals in highly uniform graphene sheets via liquid ultrasound exfoliation. In such a manner, it not only can increase the dispersion of graphene by ethyl cellulose as stabilizer,[35,36] but also can well-maintain the high conductivity of graphene.[37] As a result, compared with the device utilizing pristine ZnO ETL, the inverted solar cell based on P3HT:PC_{61}BM with a ZnO@G:EC nanocomposite ETL improves PCE from 3.3% to 3.9%. In addition, the hybrid ZnO-based ETL shows a good universality on the device based on a blend of polythieno[3,4-*b*]thiophene/benzodithiophene (PTB7) with (6,6)-phenyl-C_{71} butyric acid methyl ester (PC_{71}BM), yielding an improved PCE of 8.4%.

EXPERIMENTAL SECTION

Material Synthesis. Graphene:ethyl cellulose (G:EC) powder was synthesized by liquid ultrasound exfoliation.[35,37−39] Graphene power (200.0 mg, XFNANO Material Technologic Co. Ltd., Nanjing, China) was dispersed in an ethyl cellulose (EC) ethanol solution (2% w/v dispersion, 100 mL; EC: Aladdin, 3−7 mPa·s, 5% in toluene/ethanol 80:20) in a sebc bottle. The dispersion was sonicated utilizing a sonication system (High-power Ultrasonic Cleaner Model KQ-800 KDB) for 24 h at 60 W in a water bath. The resulting dispersion was centrifuged (Desktop High-speed Refrigerated Centrifuge Model TGL-16) at 7500 rpm for 15 min, and then the supernatant liquid was directly collected. Deionized water was mixed with the supernatant liquid (3:4 weight ratio) and subsequently centrifuged at 7500 rpm for 10 min. Thereafter, the lower precipitation was collected and dried. The resulting precipitation was redispersed in ethanol (10 mg/mL). NaCl aqueous solution (0.04 g/mL) was mixed with the redispersion (9:16 weight ratio) and centrifuged at 7500 rpm for 8 min, discarding the supernatant. To debride any residual salt, the resulting G:EC precipitation was washed with deionized water and collected by vacuum filtration (Haiyan New Oriental plastics Technology Co., Ltd. 0.45 μm filter paper). Finally, the G:EC product was dried as a fine black powder. For the zinc oxide@graphene:ethyl cellulose (ZnO@G:EC) solution preparation: The blank G:EC powder (10 mg) was dispersed in ethanol (1 mL) by bath sonication. Then the resulting liquid (10 μL) was added to a zinc oxide (ZnO) precursor solution (1 mL). Similarly, ZnO@graphene (ZnO@G) and ZnO@graphene oxide (ZnO@GO) were prepared by adopting the same preparatory procedure, excepting replacing ZnO@G:EC.

Device Fabrication. Polymeric solar cells were fabricated based on poly(3-hexylthiophene) (P3HT):(6,6)-phenyl-C_{61} butyric acid methyl ester (PC_{61}BM) with ZnO or the hybrid ZnO materials as electron transport layers (ETLs). All devices were fabricated on pretreated ITO glass substrates (sheet resistance 15 Ωsq^{-1}), cleaned sequentially using sonication in acetone, detergent, deionized water, and isopropanol, and then dried under a nitrogen stream, followed by ultraviolet light irradiation. Then the ETL (ZnO, ZnO@G, ZnO@GO, ZnO@G:EC) was spin coated and thermally annealed at 150 °C for 15 min. Thereafter, the active layer of P3HT:PC_{61}BM (1:0.8) in 1,2-dichlorobenzene was spin coated, followed by thermal annealing at 150 °C for 10 min in the glovebox. Or the band gap photoactive blend layer of PTB7 and PC_{71}BM (1:1.5 w/w, concentration of 25 mg/mL) with DIO additive (97:3, v/v) in chlorobenzene was spin coated and dried for 3 h at room temperature in the glovebox. Eventually, the double-layer structure of molybdenum trioxide (MoO_3) (7 nm)/argentum Ag (90 nm) was deposited over the active layer by thermal evaporation under a vacuum of 6×10^{-4} Torr to accomplish the device fabrication. The effective area of one cell was 0.08 cm^2. The $J-V$ curves were measured with a Keithley 2400 source meter (Abet Solar Simulator Sun2000) in the dark and under an AM 1.5G light source (100 mW cm^{-2}). All measurements were carried out under the same conditions.

General Measurements and Characterizations. The morphologies of all materials were researched by environmental scanning electron microscopy (SEM) (QuanTA-200F). The corresponding transmission scanning electron microscopy (TEM) images were characterized by JEOL-2100F transmission electron microscopy. The topography of the electron transport layer was surveyed by atomic force microscopy (AFM) (Digital Instrumental Nanoscope 31) in tapping mode. The AFM scan range is 5×5 μm^2. The corresponding ultraviolet photoelectron spectroscopy (UPS) for determining the work function was measured by AXIS-ULTRA DLD spectrometer using the He I (21.22 eV) radiation line, with an experimental resolution of 0.15 eV. The onset of photoemission of the sample was estimated using standard procedures with a −5 V bias. Survey X-ray photoelectron spectra (XPS) were investigated with a Thermo-VG Scientific ESCALAB 250 photoelectron spectrometer. Graphene materials and composites were characterized by Raman microscopy (LabRam-1B). X-ray diffraction (XRD) was measured with a copper target (λ = 1.54 Å) and a Bruker D8 focus X-ray diffractometer. The external quantum efficiency (EQE) studies were performed (Oriel Cornerstone 260 1/4 m monochromator) using calibrating incident light. In order to survey the influences of graphene materials doping on the electrical properties, the device structure of ITO/ETL/Au was fabricated. The current−voltage scans were taken within the scope of −3 to 3 V.

Electron-Only Device Measurements. To research the drift of electrons normal to the ETL's plane, the electron-only device test method was used.[40] The device configuration adopted for the measurements was ITO/ETL/Active Layer/LiF/Al. The current−voltage scans were taken within the scope of −3 to 3 V.

RESULTS AND DISCUSSION

Equal concentration of graphene, GO, and graphene:ethyl cellulose (G:EC) solution (10 mg/mL) were treated with ultrasound in ethanol for 5 min, respectively. The detailed preparation is described in the Experimental Section. The photographs of graphene, GO, and G:EC dispersed ethanol

DOI: 10.1021/acsami.5b04555
ACS Appl. Mater. Interfaces 2015, 7, 16078−16085

solutions after ultrasound treatment are shown in Figure 1a. After storage for 7 days, stratification can be found in GO

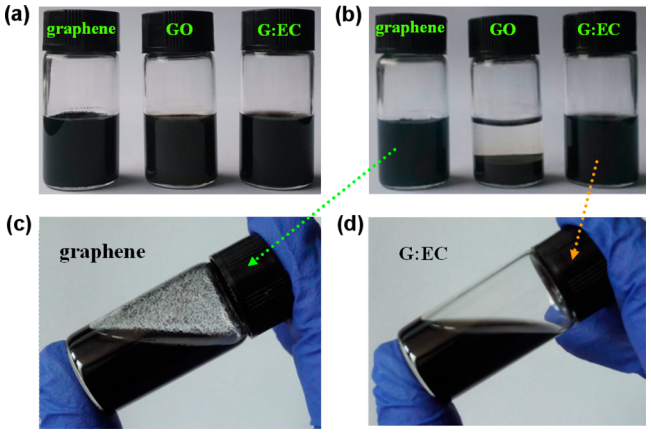

Figure 1. (a) Photographs of graphene, graphene oxide (GO), and graphene:ethyl cellulose (G:EC) disperse ethanol solutions after ultrasound treatment. (b) Photographs of graphene, GO, and G:EC ethanol solutions stored for 7 days. Tilted photographs of (c) graphene and (d) G:EC ethanol solutions stored for 7 days.

ethanol solution (Figure 1b), and evident graphene particles adhere to the sidewall in graphene ethanol solution (Figure 1c). In contrast, the G:EC dispersed ethanol solution demonstrates a highly uniform and homogeneous suspension solution (Figure 1b and Figure 1d), indicating the successful preparation of G:EC with good dispersibility.

In order to verify the degree of dispersion of exfoliated graphene by ethyl cellulose ethanol solution via liquid ultrasound exfoliation, scanning electron microscopy (SEM) and transmission electron microscopy (TEM) were performed (Figure 2). For comparison, the morphologies of the pristine graphene and RGO prepared by 150 °C thermal annealing for 15 min were also determined. All of samples were spin-coated on ITO and tested under the same testing conditions. Selected-area electron diffraction (SAED) images of graphene, RGO, and G:EC are shown in the corresponding inset. Figure 2a shows a rough morphology of the pristine graphene, and clearly stacked graphene can be seen in Figure 2d. The ring pattern in the SAED image confirms the severe aggregation of the graphene nanosheets. For the RGO, the stacking of the nanosheets, which partly cover the ITO substrate, has been obviously diminished and the dispersion of flaky RGO is also improved, as displayed in Figure 2b. Different orientations of the RGO are detected in the TEM image (Figure 2e), together with the SAED yielding messy spot patterns. Intriguingly, after treatment with ethyl cellulose ethanol solution via liquid ultrasound exfoliation, graphene nanosheets can fully cover and tightly attach on the ITO substrate with a quite smooth surface morphology (Figure 2c). Figure 2f displays an individual graphene sheet with six spot patterns in the SAED of G:EC, suggesting that G:EC is scattered as individual graphene-based sheets.[41] The Raman spectra of graphene, RGO, and G:EC also reveal consistent results in Figure S1.

Then, those 2D graphene materials were employed to act as a matrix for in situ preparation of a ZnO film. The Raman spectra of bare ZnO and hybrid ZnO materials are shown in Figure S2a. An obvious graphene characteristic peak at 1584 cm^{-1} can be observed after incorporation of a carbon matrix. The intensity and position of that peak have no significant change with various volume fractions of G:EC in Figure S2b. In addition, X-ray photoelectron spectra (XPS) measurement was applied to in situ formation of a zinc oxide@graphene:ethyl cellulose (ZnO@G:EC) film, as shown in Figure S3. It is evident that Zn $2p_{1/2}$ peak centers at 1044.4 eV and Zn $2p_{3/2}$ centers at 1021.2 eV for both pristine ZnO and ZnO@G:EC films. Then, the X-ray diffraction (XRD) of ZnO and ZnO@G:EC samples has been measured to characterize ZnO (Figure S4). No distinct peaks can be seen for ZnO, which is consistent with previous reports.[42] This can be attributed to in situ formation of ZnO being amorphous. For ZnO@G:EC, the typical diffraction peak of graphene appeared at $2\theta = 26.2°$. The in situ growth of ZnO nanocrystals in the G:EC matrix can be further verified by TEM and SEM images. The pristine ZnO nanocrystals are sparsely decentralized on the substrate (Figure 3a and Figure S5a), while heterogeneous ZnO nanocrystals tend to aggregate atop the thick and rugged graphene sheets for

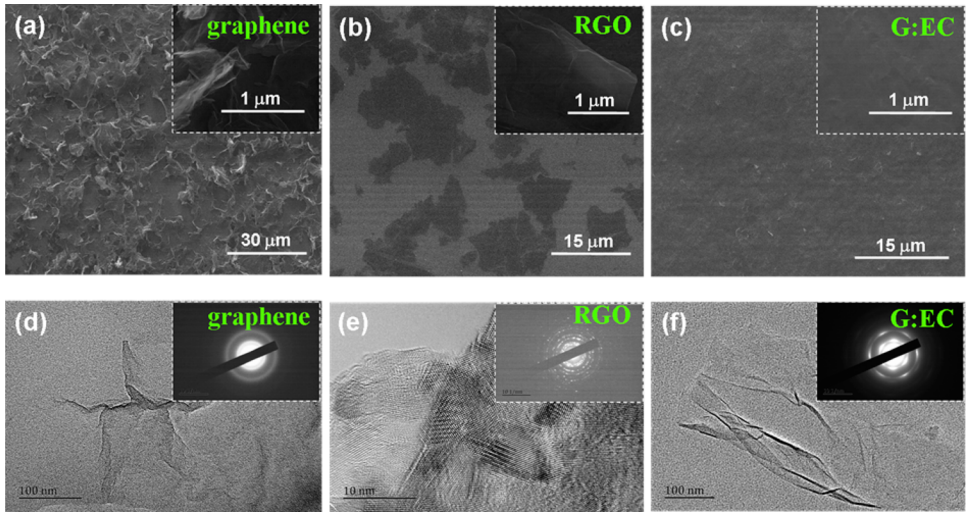

Figure 2. Low-magnification scanning electron microscopy (SEM) images of (a) graphene, (b) reduced graphene oxide (RGO), and (c) G:EC; the insets show a high-magnification SEM image of the corresponding image. Transmission electron microscopy (TEM) images of (d) graphene, (e) RGO, and (f) G:EC; the insets show a selected-area electron diffraction pattern of the corresponding image.

DOI: 10.1021/acsami.5b04555
ACS Appl. Mater. Interfaces 2015, 7, 16078−16085

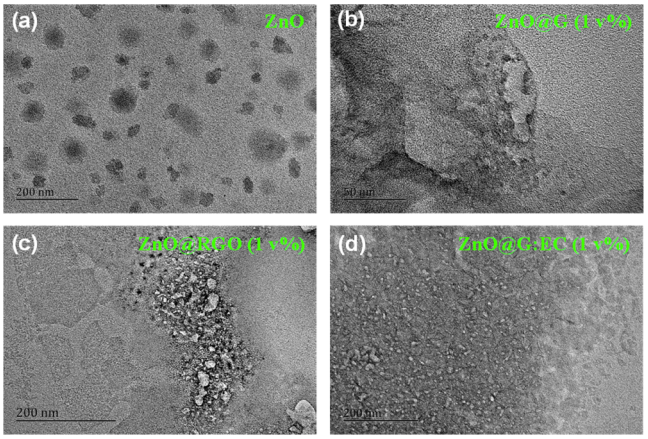

Figure 3. TEM images of (a) zinc oxide (ZnO), (b) ZnO@graphene (ZnO@G) (1 vol %), (c) ZnO@reduced graphene oxide (ZnO@RGO) (1 vol %), and (d) ZnO@graphene:ethyl cellulose (ZnO@G:EC) (1 vol %). The 10 μL of graphene (GO and G:EC) ethanol solution was dispersed in 1 mL of ZnO precursor solution to obtain 1 vol % of ZnO@G (ZnO@graphene oxide (ZnO@GO) and ZnO@G:EC) solution.

the ZnO@graphene (ZnO@G) (1 vol %) film (Figure 3b and Figure S5b), which is consistent with the strong stack of graphene (Figure 2d). The 10 μL of graphene (GO and G:EC) ethanol solution was dispersed in 1 mL of ZnO precursor solution to obtain 1 vol % of ZnO@G (ZnO@graphene oxide (ZnO@GO) and ZnO@G:EC) solution. Similarly, ZnO nanocrystals aggregate significantly on the top of some flaky RGO in the ZnO@reduced graphene oxide (ZnO@RGO) (1 vol %) film (Figure 3c and Figure S5c), due to the insufficient adhesion area for deposition of ZnO nanocrystals. The aggregation of ZnO nanocrystals could form more recombination centers at the interfacial contact, resulting in a poor device performance. Delightfully, in situ formation of ZnO nanocrystals occurs evenly and compactly on the consecutive graphene sheets in the ZnO@G:EC (1 vol %) film (Figure 3d and Figure S 5d). The morphology of the various ETLs was further investigated by atomic force microscopy (AFM). As shown in Figure 4, for a pristine ZnO film, the maximum height is 17 nm (Figure 4a); nevertheless, the value of a ZnO@G (1 vol %) film increases to 19 nm (Figure 4b), still for the stack of graphene on a film surface. For the ZnO-loaded RGO film, the maximum height is slightly reduced to 16 nm (Figure 4c). Compared with the three mentioned films, the ZnO@G:EC (1 vol %) film reveals the smoothest morphology with a 14 nm maximum height (Figure 4d), which could contribute to the improvement of electron extraction. Different images of the volume fraction of G:EC in ZnO precursor solution are exhibited in Figure S6, and it is clearly found that the films become rougher when the volume fraction of G:EC is over 1 vol %. Thus, ZnO@G:EC (1 vol %) film is employed as ETLs for devices fabrication.

Since the graphene in ZnO@G:EC films is physically dispersed by EC, the electric property is expected to be well maintained. Therefore, the conductivity of ETLs was measured in Figure 5a. It is obvious that all hybrid ZnO composites exhibit a better conductivity than the bare ZnO (1.15×10^{-4} cm^{-1} Ω^{-1}), thanks to incorporation of the high conductive graphene. As expected, compared with the ZnO@RGO (1.70×10^{-4} cm^{-1} Ω^{-1}), the ZnO@G:EC (1 vol %) film demonstrates the much higher conductivity of 2.19×10^{-4} cm^{-1} Ω^{-1}. Note

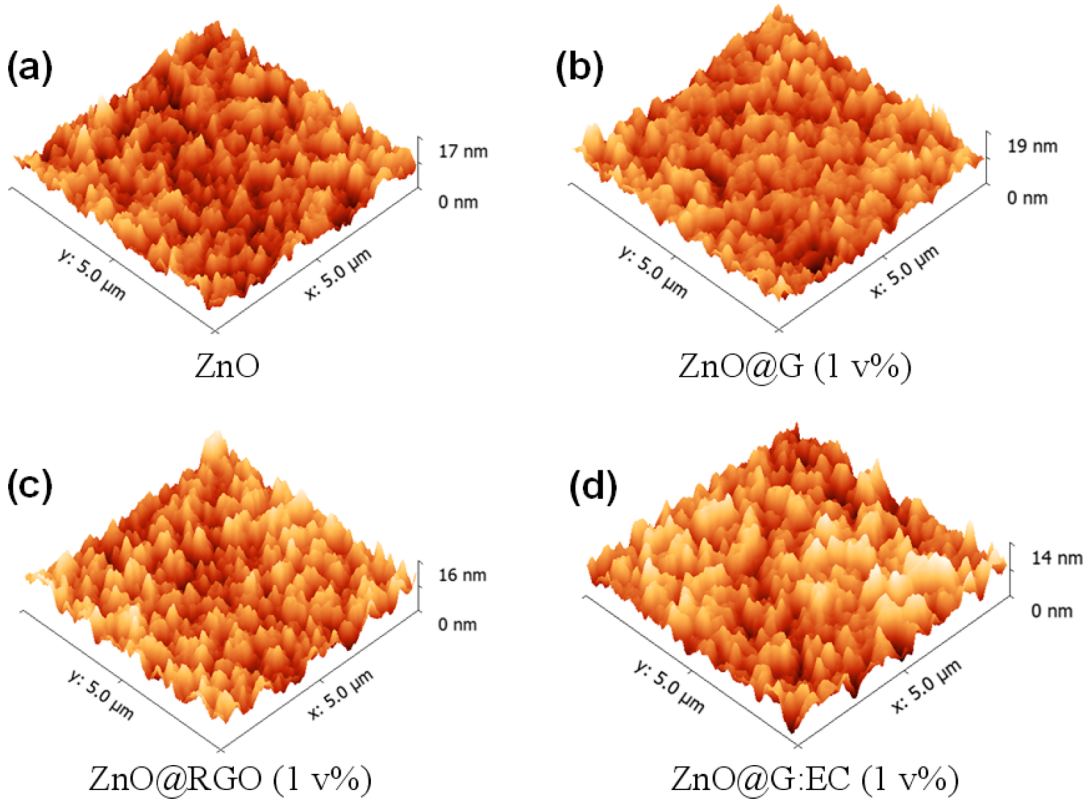

Figure 4. Atomic force microscopy (AFM) micrographs of the morphologies of different electron transport layer materials on top of the ITO: (a) ZnO, (b) ZnO@G (1 vol %), (c) ZnO@RGO (1 vol %), (d) ZnO@G:EC (1 vol %).

DOI: 10.1021/acsami.5b04555
ACS Appl. Mater. Interfaces 2015, 7, 16078−16085

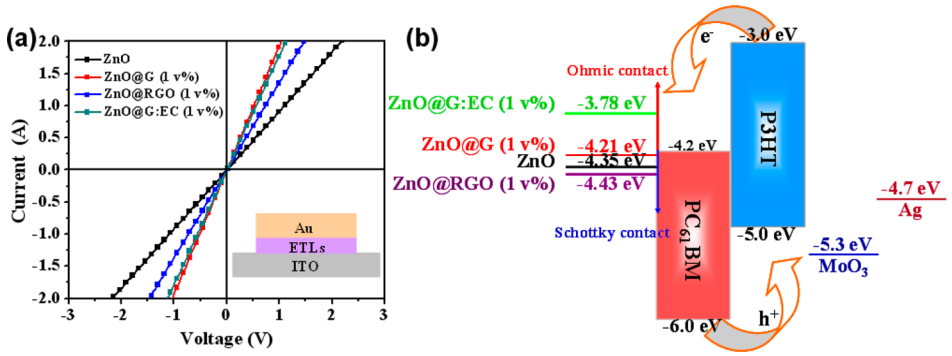

Figure 5. (a) *I*–*V* curves for electron-only transfer devices, (b) band diagram of the device and electrical contacts of the work function of cathodes with the LUMO level of $PC_{61}BM$.

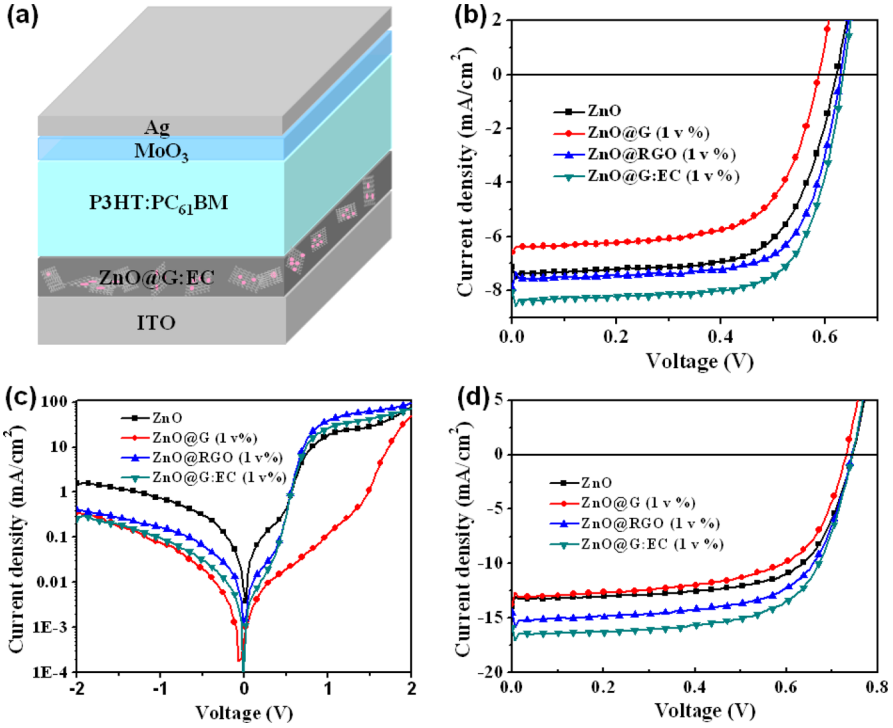

Figure 6. (a) Device structure, (b) *J*–*V* curves of the PSC devices based on poly(3-hexylthiophene) (P3HT):(6,6)-phenyl-C_{61} butyric acid methyl ester ($PC_{61}BM$) with four different materials (ZnO, ZnO@G (1 vol %), ZnO@RGO (1 vol %), ZnO@G:EC (1 vol %)) as electron transport layer, (c) *J*–*V* curves in the dark. (d) *J*–*V* curves of the PSC devices based on polythieno[3,4-*b*]thiophene/benzodithiophene (PTB7):(6,6)-phenyl-C_{71} butyric acid methyl ester ($PC_{71}BM$) with four different materials (ZnO, ZnO@G (1 vol %), ZnO@RGO (1 vol %), ZnO@G:EC (1 vol %)) as electron transport layer.

Table 1. Device Parameters of the PSCs with Different Electron Transport Layers (ETLs) and Active Layers under the Illumination of AM 1.5G, 100 mW cm^{-2}

ETLs	Active layers	J_{sc} (mA cm^{-2})	V_{oc} (V)	FF	PCE (%)
ZnO	P3HT:$PC_{61}BM$	7.15 ± 0.46 (6.52)[c]	0.62 ± 0.01	0.69 ± 0.02	3.1 (3.3)[b]
ZnO@G (1 vol %)	P3HT:$PC_{61}BM$	6.57 ± 0.55 (6.39)[c]	0.59 ± 0.02	0.63 ± 0.03	2.4 (2.7)[b]
ZnO@RGO (1 vol %)	P3HT:$PC_{61}BM$	7.91 ± 0.53 (6.99)[c]	0.63 ± 0.01	0.67 ± 0.02	3.3 (3.4)[b]
ZnO@G:EC (1 vol %)	P3HT:$PC_{61}BM$	8.05 ± 0.55 (7.73)[c]	0.63 ± 0.01	0.73 ± 0.02	3.7 (3.9)[b]
ZnO	PTB7: $PC_{71}BM$	13.95 ± 0.51(13.78)[c]	0.74 ± 0.01	0.63 ± 0.02	6.5 (6.7)[b]
ZnO@G (1 vol %)	PTB7: $PC_{71}BM$	13.76 ± 0.58(13.52)[c]	0.73 ± 0.01	0.59 ± 0.03	6.0 (6.2)[b]
ZnO@RGO (1 vol %)	PTB7: $PC_{71}BM$	14.49 ± 0.55(13.89)[c]	0.74 ± 0.01	0.68 ± 0.02	7.3 (7.6)[b]
ZnO@G:EC (1 vol %)	PTB7: $PC_{71}BM$	15.88 ± 0.60(15.61)[c]	0.74 ± 0.01	0.69 ± 0.03	8.1(8.4)[b]

[a]All values represent averages from 50 devices on a single chip, and the areas were tested with an aperture. [b]The best PCE. The effective area of one cell was 0.08 cm^2. [c]The calculated J_{sc} value, according to EQE spectra.

that the insulating EC molecule in the ZnO@G:EC exerts little impact on the electric property of the film, as supported by the almost identical conductivity of ZnO@G (2.43 × 10^{-4} cm^{-1} Ω^{-1}) and ZnO@G:EC. The admirable conductivity of the

DOI: 10.1021/acsami.5b04555
ACS Appl. Mater. Interfaces 2015, 7, 16078–16085

ZnO@G:EC (1 vol %) composite could render a PSCs device to deliver a superior device performance.

The inverted PSCs devices with ETLs of pristine ZnO and hybrid ZnO were fabricated to evaluate their effects on device performance. The energy band schematic diagram for the PSCs and the device structure are demonstrated in Figure 5b and Figure 6a, respectively. The energy bands of different ETLs are described according to ultraviolet photoelectron spectroscopy (UPS) spectra. The UPS spectra are shown in Figure S7, and the work function is illustrated in Table S1. Replacing the pure ZnO with the ZnO@G:EC (1 vol %) composite, the work function decreases to 3.78 eV. The decreased work function can be propitious to the electron extraction and transportation from the active layer to the ETL of ZnO@G:EC (1 vol %). In addition, UPS spectra of ZnO@G:EC with various volume fractions are also presented in Figure S8, and the corresponding work functions are listed in Table S2. Obviously, the work function of ZnO@G:EC (1 vol %) is more suitable as cathode buffer layer compared with that of ZnO@G:EC with other volume fractions.

The current density versus voltage ($J-V$) curves of the inverted devices under illumination and in the dark are displayed in Figure 6b and Figure 6c, and the corresponding parameters are summarized in Table 1. Compared with the device of poly(3-hexylthiophene) (P3HT):(6,6)-phenyl-C_{61} butyric acid methyl ester ($PC_{61}BM$) with bare ZnO as ETL yielding a PCE of 3.1%, the device with ZnO@G (1 vol %) shows significantly reduced efficiency of 2.4% (Figure 6b). This is presumably ascribed to the aggregation of ZnO on the stacked graphene sheets (Figure 3b). When the devices based on ZnO films are modified with RGO as ETL, PCE is improved to 3.3%, owing to the optimized morphology of the ZnO@RGO (1 vol %) (Figure 4c). Further replacing the ETL with ZnO@G:EC (1 vol %), a best PCE of 3.7% has been achieved with the enhanced J_{sc} of 8.05 mA cm^{-2} and a FF of 73%. The improvement in PCE is related to the high conductive graphene and the smoothest morphology originating from EC stabilizer effectively impeding aggregation of graphene (Figure 4d), facilitating the charge transportation and reducing charge recombination. The improved current is matched up with the external quantum efficiency (EQE) spectra that can estimate the J_{sc} value (Figure S9). The considerable smaller leakage current of the device with ZnO@G:EC (1 vol %) as ETL also hints at the decreased charge recombination in the ZnO@G:EC (1 vol %) ETL (Figure 6c).[43,44] And the shunt resistance of the device with ZnO@G:EC (1 vol %) increases compared to the device with ZnO@RGO (1 vol %). In addition, the V_{oc} is slightly higher than that of the bare ZnO based device, in accordance with the UPS observation.

To further verify the universality of in situ formation of ZnO nanocrystal interfacial layers in a graphene matrix in PSCs, we single out a blend of high-performance low-bandgap polymer polythieno[3,4-*b*]thiophene/benzodithiophene (PTB7) with (6,6)-phenyl-C_{71} butyric acid methyl ester ($PC_{71}BM$) as the active layer in PSCs. The $J-V$ curves of the device based on the PTB7:$PC_{71}BM$ blend are displayed in Figure 6d, and the device parameters as well as corresponding calculated J_{sc} values are summarized in Table 1. Among these devices with ZnO, ZnO@G (1 vol %), ZnO@RGO (1 vol %), or ZnO@G:EC (1 vol %), the one with ZnO@G:EC (1 vol %) exhibits the best PCE (8.1%) with a V_{oc} of 0.74 V, a J_{sc} of 15.88 mA/cm^2, and a FF of 69% (Table 1), which is obviously superior to the PCE of the normal device with the ZnO ETL (6.5%). The corresponding PCE histogram of devices with ZnO@G:EC (1 vol %) as ETL shows that the maximum PCE can be up to 8.4% in Figure S10. Similarly to the results from the P3HT:$PC_{61}BM$ devices, the improvements in the PCE are mainly attributed to the improved J_{sc} and conductivity, which indicates this novel ZnO@G:EC cathode buffer layer is quite universal.

CONCLUSIONS

The ZnO@G:EC (1 vol %) nanocomposite was prepared by in situ formation of ZnO nanocrystals in the uniformly distributed graphene matrix for high performance polymer solar cells. The method of exfoliating graphene in EC ethanol solution not only can be conducive to homogeneous distribution of graphene by EC as stabilizer but also well-maintains the high conductivity of graphene. Compared with a pure ZnO cathode buffer layer, ZnO@G:EC possesses higher conductivity, smoother morphology, and lower work function, which can boost the electron transport and extraction between the cathode and the active layer and reduce carrier recombination. It can be found that incorporation of the ZnO@G:EC (1 vol %) nanocomposite as cathode buffer layer can effectively improve the PCE of the inverted device, based on a PCE value of 3.9% with P3HT:$PC_{61}BM$. Moreover, a further optimized PCE of 8.4% has been realized in the device based on PTB7:$PC_{71}BM$ as the active layer. The results reveal that ZnO@G:EC is simply applicable as ETL for optimizing PSCs performance.

ASSOCIATED CONTENT

Supporting Information

Raman spectra, X-ray photoelectron spectra, X-ray diffraction patterns, scanning electron microscopy images, atomic force microscopy micrographs, ultraviolet photoelectron spectroscopy spectra, derived work function data of the hybrid graphene nanocomposites, and external quantum efficiency spectra and histogram of power conversion efficiency of photovoltaic devices based on P3HT:$PC_{61}BM$ and PTB7:$PC_{71}BM$. The Supporting Information is available free of charge on the ACS Publications website at DOI: 10.1021/acsami.5b04555.

AUTHOR INFORMATION

Corresponding Author

*Tel.: +86 791 83968703. Fax: +86 791 83969561. E-mail: ywchen@ncu.edu.cn (Y. Chen).

Author Contributions

Aifeng Hu and Lie Chen contributed equally to this work.

Notes

The authors declare no competing financial interest.

ACKNOWLEDGMENTS

This work was financially supported by the National Science Fund for Distinguished Young Scholars (51425304), National Natural Science Foundation of China (51273088, 51263016, and 51473075), and National Basic Research Program of China (973 Program 2014CB260409).

REFERENCES

(1) He, Z.; Xiao, B.; Liu, F.; Wu, H.; Yang, Y.; Xiao, S.; Wang, C.; Russell, T. P.; Cao, Y. Single-Junction Polymer Solar Cells with High Efficiency and Photovoltage. *Nat. Photonics* **2015**, *9*, 174−179.

(2) Kuang, C.; Tang, G.; Jiu, T.; Yang, H.; Liu, H.; Li, B.; Luo, W.; Li, X.; Zhang, W.; Lu, F. Highly Efficient Electron Transport Obtained by

DOI: 10.1021/acsami.5b04555
ACS Appl. Mater. Interfaces 2015, 7, 16078−16085

Doping PCBM with Graphdiyne in Planar-Heterojunction Perovskite Solar Cells. *Nano Lett.* **2015**, *15*, 2756−2762.
(3) Chen, L.-M.; Hong, Z.; Li, G.; Yang, Y. Recent Progress in Polymer Solar Cells: Manipulation of Polymer:Fullerene Morphology and the Formation of Efficient Inverted Polymer Solar Cells. *Adv. Mater.* **2009**, *21*, 1434−1449.
(4) De Jong, M. P.; Van Ijzendoorn, L. J.; De Voigt, M. J. A. Stability of the Interface between Indium-Tin-Oxide and Poly(3,4-ethylenedioxythiophene)/Poly(styrenesulfonate) in Polymer Light-Emitting Diodes. *Appl. Phys. Lett.* **2000**, *77*, 2255 (1−3).
(5) Jørgensen, M.; Norrman, K.; Krebs, F. C. Stability/Degradation of Polymer Solar Cells. *Sol. Energy Mater. Sol. Cells* **2008**, *92*, 686−714.
(6) He, Z.; Zhong, C.; Su, S.; Xu, M.; Wu, H.; Cao, Y. Enhanced Power-Conversion Efficiency in Polymer Solar Cells Using an Inverted Device Structure. *Nat. Photonics* **2012**, *6*, 591−595.
(7) Lee, B. R.; Jung, E. D.; Nam, Y. S.; Jung, M.; Park, J. S.; Lee, S.; Choi, H.; Ko, S. J.; Shin, N. R.; Kim, Y. K.; Kim, S. O.; Kim, J. Y.; Shin, H. J.; Cho, S.; Song, M. H. Amine-Based Polar Solvent Treatment for Highly Efficient Inverted Polymer Solar Cells. *Adv. Mater.* **2014**, *26*, 494−500.
(8) Sharma, G. D.; Keshtov, M. L.; Khokhlov, A. R.; Tasis, D.; Galiotis, C. Improved Power Conversion Efficiency by Insertion of RGO-TiO_2 Composite Layer as Optical Spacer in Polymer Bulk Heterojunction Solar Cells. *Org. Electron.* **2014**, *15*, 348−355.
(9) You, J.; Chen, C. C.; Dou, L.; Murase, S.; Duan, H. S.; Hawks, S. A.; Xu, T.; Son, H. J.; Yu, L.; Li, G.; Yang, Y. Metal Oxide Nanoparticles as an Electron-Transport Layer in High-Performance and Stable Inverted Polymer Solar Cells. *Adv. Mater.* **2012**, *24*, 5267−5272.
(10) Brabec, C. J.; Shaheen, S. E.; Winder, C.; Sariciftci, N. S.; Denk, P. Effect of LiF/Metal Electrodes on the Performance of Plastic Solar Cells. *Appl. Phys. Lett.* **2002**, *80*, 1288 (1−3).
(11) Padinger, F.; Rittberger, R. S.; Sariciftci, N. S. Effects of Postproduction Treatment on Plastic Solar Cells. *Adv. Funct. Mater.* **2003**, *13*, 85−88.
(12) Shaheen, S. E.; Brabec, C. J.; Sariciftci, N. S.; Padinger, F.; Fromherz, T.; Hummelen, J. C. 2.5% Efficient Organic Plastic Solar Cells. *Appl. Phys. Lett.* **2001**, *78*, 841 (1−3).
(13) Beliatis, M. J.; Gandhi, K. K.; Rozanski, L. J.; Rhodes, R.; McCafferty, L.; Alenezi, M. R.; Alshammari, A. S.; Mills, C. A.; Jayawardena, K. D.; Henley, S. J.; Silva, S. R. Hybrid Graphene-Metal Oxide Solution Processed Electron Transport Layers for Large Area High-Performance Organic Photovoltaics. *Adv. Mater.* **2014**, *26*, 2078−2083.
(14) Ji, Z.; Wu, R.; Adamska, L.; Velizhanin, K. A.; Doorn, S. K.; Sykora, M. In Situ Synthesis of Graphene Molecules on TiO_2: Application in Sensitized Solar Cells. *ACS Appl. Mater. Interfaces* **2014**, *6*, 20473−20478.
(15) Dkhil, S. B.; Duché, D.; Gaceur, M.; Thakur, A. K.; Aboura, F. B.; Escoubas, L.; Simon, J.-J.; Guerrero, A.; Bisquert, J.; Garcia-Belmonte, G.; Bao, Q.; Fahlman, M.; Videlot-Ackermann, C.; Margeat, O.; Ackermann, J. Interplay of Optical, Morphological, and Electronic Effects of ZnO Optical Spacers in Highly Efficient Polymer Solar Cells. *Adv. Energy Mater.* **2014**, *4*, 1400805 (1−12).
(16) Woo Lee, H.; Young Oh, J.; Il Lee, T.; Soon Jang, W.; Bum Yoo, Y.; Sang Chae, S.; Ho Park, J.; Min Myoung, J.; Moon Song, K.; Koo Baik, H. Highly Efficient Inverted Polymer Solar Cells with Reduced Graphene-Oxide-Zinc-Oxide Nanocomposites Buffer Layer. *Appl. Phys. Lett.* **2013**, *102*, 193903 (1−4).
(17) Li, P.; Jiu, T.; Tang, G.; Wang, G.; Li, J.; Li, X.; Fang, J. Solvents Induced ZnO Nanoparticles Aggregation Associated with Their Interfacial Effect on Organic Solar Cells. *ACS Appl. Mater. Interfaces* **2014**, *6*, 18172−18179.
(18) Roest, A. L.; Kelly, J. J.; Vanmaekelbergh, D.; Meulenkamp, E. A. Staircase in the Electron Mobility of a ZnO Quantum Dot Assembly due to Shell Filling. *Phys. Rev. Lett.* **2002**, *89*, 036801 (1−4).
(19) Xie, C.; Chen, L.; Chen, Y. Electrostatic Self-Assembled Metal Oxide/Conjugated Polyelectrolytes as Electron-Transporting Layers for Inverted Solar Cells with High Efficiency. *J. Phys. Chem. C* **2013**, *117*, 24804−24814.
(20) Sakohara, S.; Ishida, M.; Anderson, M. A. Visible Luminescence and Surface Properties of Nanosized ZnO Colloids Prepared by Hydrolyzing Zinc Acetate. *J. Phys. Chem. B* **1998**, *102*, 10169−10175.
(21) Monticone, S.; Tufeu, R.; Kanaev, A. Complex Nature of the UV and Visible Fluorescence of Colloidal ZnO Nanoparticles. *J. Phys. Chem. B* **1998**, *102*, 2854−2862.
(22) Hau, S. K.; Yip, H.-L.; Baek, N. S.; Zou, J.; O'Malley, K.; Jen, A. K. Y. Air-Stable Inverted Flexible Polymer Solar Cells Using Zinc Oxide Nanoparticles as an Electron Selective Layer. *Appl. Phys. Lett.* **2008**, *92*, 253301 (1−3).
(23) Kyaw, A. K. K.; Sun, X. W.; Jiang, C. Y.; Lo, G. Q.; Zhao, D. W.; Kwong, D. L. An Inverted Organic Solar Cell Employing a Sol-Gel Derived ZnO Electron Selective Layer and Thermal Evaporated MoO_3 Hole Selective Layer. *Appl. Phys. Lett.* **2008**, *93*, 221107 (1−3).
(24) Faÿ, S.; Kroll, U.; Bucher, C.; Vallat-Sauvain, E.; Shah, A. Low Pressure Chemical Vapour Deposition of ZnO Layers for Thin-film Solar Cells: Temperature-Induced Morphological Changes. *Sol. Energy Mater. Sol. Cells* **2005**, *86*, 385−397.
(25) Zhou, Z.; Kato, K.; Komaki, T.; Yoshino, M.; Yukawa, H.; Morinaga, M. Effects of Hydrogen Doping through Ion Implantation on the Electrical Conductivity of ZnO. *Int. J. Hydrogen Energy* **2004**, *29*, 323−327.
(26) Zhou, Z.; Kato, K.; Komaki, T.; Yoshino, M.; Yukawa, H.; Morinaga, M.; Morita, K. Effects of Dopants and Hydrogen on the Electrical Conductivity of ZnO. *J. Eur. Ceram. Soc.* **2004**, *24*, 139−146.
(27) Nakamura, A.; Temmyo, J. Schottky Contact on ZnO Nano-Columnar Film with H_2O_2 Treatment. *J. Appl. Phys.* **2011**, *109*, 093517 (1−7).
(28) Schifano, R.; Monakhov, E.; Grossner, U.; Svensson, B. Electrical Characteristics of Palladium Schottky Contacts to Hydrogen Peroxide Treated Hydrothermally Grown ZnO. *Appl. Phys. Lett.* **2007**, *91*, 193507 (1−7).
(29) Eita, M.; Labban, A. E.; Cruciani, F.; Usman, A.; Beaujuge, P. M.; Mohammed, O. F. Ambient Layer-by-Layer ZnO Assembly for Highly Efficient Polymer Bulk Heterojunction Solar Cells. *Adv. Funct. Mater.* **2015**, *25*, 1558−1564.
(30) Barpuzary, D.; Qureshi, M. Enhanced Photovoltaic Performance of Semiconductor-Sensitized ZnO-CdS Coupled with Graphene Oxide as a Novel Photoactive Material. *ACS Appl. Mater. Interfaces* **2013**, *5*, 11673−11682.
(31) Tung, V. C.; Kim, J.; Huang, J. Graphene Oxide:Single-Walled Carbon Nanotube-Based Interfacial Layer for All-Solution-Processed Multijunction Solar Cells in Both Regular and Inverted Geometries. *Adv. Energy Mater.* **2012**, *2*, 299−303.
(32) Hu, T.; Chen, L.; Yuan, K.; Chen, Y. Poly(N-vinylpyrrolidone)-Decorated Reduced Graphene Oxide with ZnO Grown in Situ as a Cathode Buffer Layer for Polymer Solar Cells. *Chem. - Eur. J.* **2014**, *20*, 17178−17184.
(33) Jayawardena, K. D. G. I.; Rhodes, R.; Gandhi, K. K.; Prabhath, M. R. R.; Dabera, G. D. M. R.; Beliatis, M. J.; Rozanski, L. J.; Henley, S. J.; Silva, S. R. P. Solution Processed Reduced Graphene Oxide/Metal Oxide Hybrid Electron Transport Layers for Highly Efficient Polymer Solar Cells. *J. Mater. Chem. A* **2013**, *1*, 9922−9927.
(34) Hu, Y. H.; Wang, H.; Hu, B. Thinnest Two-Dimensional Nanomaterial-Graphene for Solar Energy. *ChemSusChem* **2010**, *3*, 782−796.
(35) Liang, Y. T.; Hersam, M. C. Highly Concentrated Graphene Solutions via Polymer Enhanced Solvent Exfoliation and Iterative Solvent Exchange. *J. Am. Chem. Soc.* **2010**, *132*, 17661−17663.
(36) Secor, E. B.; Lim, S.; Zhang, H.; Frisbie, C. D.; Francis, L. F.; Hersam, M. C. Gravure Printing of Graphene for Large-Area Flexible Electronics. *Adv. Mater.* **2014**, *26*, 4533−4538.
(37) Secor, E. B.; Prabhumirashi, P. L.; Puntambekar, K.; Geier, M. L.; Hersam, M. C. Inkjet Printing of High Conductivity, Flexible Graphene Patterns. *J. Phys. Chem. Lett.* **2013**, *4*, 1347−1351.

DOI: 10.1021/acsami.5b04555
ACS Appl. Mater. Interfaces 2015, 7, 16078−16085

(38) Khan, U.; O'Neill, A.; Lotya, M.; De, S.; Coleman, J. N. High-Concentration Solvent Exfoliation of Graphene. *Small* **2010**, *6*, 864−871.
(39) Secor, E. B.; Lim, S.; Zhang, H.; Frisbie, C. D.; Francis, L. F.; Hersam, M. C. Gravure Printing of Graphene for Large-Area Flexible Electronics. *Adv. Mater.* **2014**, *26*, 4533−4538.
(40) Steyrleuthner, R.; Bange, S.; Neher, D. Reliable Electron-Only Devices and Electron Transport in N-Type Polymers. *J. Appl. Phys.* **2009**, *105*, 064509 (1−8).
(41) Stankovich, S.; Dikin, D. A.; Dommett, G. H.; Kohlhaas, K. M.; Zimney, E. J.; Stach, E. A.; Piner, R. D.; Nguyen, S. T.; Ruoff, R. S. Graphene-Based Composite Materials. *Nature* **2006**, *442*, 282−286.
(42) Sun, Y.; Seo, J. H.; Takacs, C. J.; Seifter, J.; Heeger, A. J. Inverted Polymer Solar Cells Integrated with a Low-Temperature-Annealed Sol-Gel-Derived ZnO Film as an Electron Transport Layer. *Adv. Mater.* **2011**, *23*, 1679−1683.
(43) Hao, Y.; Song, J.; Yang, F.; Hao, Y.; Sun, Q.; Guo, J.; Cui, Y.; Wang, H.; Zhu, F. Improved Performance of Organic Solar Cells by Incorporating Silica-Coated Silver Nanoparticles in the Buffer Layer. *J. Mater. Chem. C* **2015**, *3*, 1082−1090.
(44) Li, S.; Li, W.; Liu, Q.; Wei, H.; Jin, E.; Wang, H.; Dong, Y.; Lu, H.; Zhang, X.; Zhao, X. Spin-Coated Ag Nanoparticles onto ITO Substrates for Efficient Improvement of Polymer Solar Cell Performance. *J. Mater. Chem. C* **2015**, *3*, 1319−1324.

DOI: 10.1021/acsami.5b04555
ACS Appl. Mater. Interfaces 2015, 7, 16078−16085